Learning to Deblur Adaptive Optics Retinal Images

Anfisa Lazareva [1*], Muhammad Asad [2], Greg Slabaugh [2]

[1] Department of Electrical and Electronic Engineering, City, University of London, London, UK
anfisa.lazareva.1@city.ac.uk
[2] Department of Computer Science, City, University of London, London, UK

Abstract. In this paper we propose a blind deconvolution approach for reconstruction of Adaptive Optics (AO) high-resolution retinal images. The framework employs Random Forest to learn the mapping of retinal images onto the space of blur kernels expressed in terms of Zernike coefficients. A specially designed feature extraction technique allows inference of blur kernels for retinal images of various quality, taken at different locations of the retina. This model is validated on synthetically generated images as well as real AO high-resolution retinal images. The obtained results on the synthetic data showed an average root-mean-square error of 0.0051 for the predicted blur kernels and 0.0464 for the reconstructed images, compared to the ground truth (GT). The assessment of the reconstructed AO retinal images demonstrated that the contrast, sharpness and visual quality of the images have been significantly improved.

Keywords: Adaptive Optics imaging, deconvolution, image restoration, regression, Random Forest

1 Introduction

Direct observation of the retina suffers from various optical aberrations of the eye. A wavefront sensor in an AO instrument performs calculation and compensation of high-order ocular aberrations thus providing a high level of resolution when imaging the retina. Despite this, due to hardware limitations of the wavefront corrector, this correction is not perfect. Therefore, the acquired retinal images are still corrupted by residual aberrations resulting in blur. Enhancement of the retinal images facilitates better distinction of photoreceptor cells and thereby assists clinicians in the examination of living retina, allowing for more accurate quantitative analysis of photoreceptor cell packing density. Additional improvements in the contrast and resolution of retinal images can be obtained *a posteriori*, by using an image restoration technique such as image deconvolution. In AO, the degradation function of the system can be estimated partially from wavefront sensing (WFS), assuming that the measurements of the deformable mirror are accurate [1]. Based on the information about the residual errors after AO correction, the system's point spread function (PSF) can be reconstructed and employed in the deconvolution process [2]. However, the WFS is not a reliable

source of data due to multiple types of noise in the AO imaging system as well as the unsynchronized process of image capturing and wavefront calculation. As a result, the obtained WFS data does not always correspond to the acquired set of frames. Therefore, ordinary deconvolution from WFS is not a suitable method for post-processing of AO images [1].

When the PSF is not available, 'blind' deconvolution, a more generalized technique, can be applied to the images. This type of image deconvolution allows for recovery of the object and the PSF distributions simultaneously from a series of measurements. This is made by the use of physical constraints about the target and knowledge of the imaging system [3]. A few blind deconvolution methods have been reported in the literature for restoring AO high-resolution retinal images [4–6]. However, conventional blind deconvolution has a drawback of getting trapped in local minima that makes it hard to find a unique solution, especially when there is only a single blurred image to be restored [1].

In this paper, we propose an image deconvolution method based on a multi-variate Random Forest regressor. Although a number of learning-based techniques have been proposed in the literature for the purposes of image deconvolution [7], [8], these methods rely on generalized models and therefore their accuracy is limited to specific types of blur. In addition, in most of the reported methods the achieved resolution of the recovered blur kernel is often found to be restricted by size. In our work, the proposed framework is specifically designed for deconvolution of retinal images acquired with a commercially available flood-illuminated AO instrument (rtx1, Imagine Eyes, Orsay, France). The blur kernel is modeled by the physics/optics of the AO system and thus constrained as a member in a class of parametric functions. This allows to significantly reduce the space of valid PSFs. A convolution kernel is estimated through non-linear regression of retinal images onto the space of PSFs expressed in terms of Zernike coefficients. By performing regression on a compact representation of the PSF, we are able to infer a convolution blur kernel for AO retinal images without compromising the resolution of the PSF. The feature extraction technique is specially developed to allow for better generalization on a large set of retinal images. To our knowledge, learning-based methods have not been previously used for AO retinal images.

2 Method

2.1 Image Model

Many tasks in image processing can be formulated as a regression problem where we learn a mapping function $f_w: X \to Y$ from the input space X to the output space Y, which is parametrized by a learned parameter w [7]. The task of image deconvolution requires estimation of original image X from its degraded observations Y obtained as a result of convolution with the system's PSF w and an additive noise n. In that sense, the imaging process can be expressed as follows:

$$Y = X * w + n\,. \tag{1}$$

Given that, the GT is provided in the form of training data T composed of input and output image pairs (X_i, Y_i^{GT}), learning the optimal convolution kernel w^* can be generally formulated using the principle of empirical risk minimization:

$$w^* = \underset{w}{\operatorname{argmin}} \sum_{i=1}^{N} \left\| Y_i^{GT} - X_i * w \right\|^2, \tag{2}$$

where N is a total number of samples.

We propose solving this problem with Random Forest, where optimal convolution kernel w^* is found through non-linear regression of blurred images $\{Y_i^{GT}\}$ onto the space of system's PSFs $\{w_i\}$. In this work, the PSFs of AO system $\{w_i\}$ are defined by the vectors of Zernike coefficients $\{\boldsymbol{a}_i\}$ and the blurred images are represented by Histograms of oriented Gradients (HoG) $\{\boldsymbol{H}_i\}$ [9]. Then, with the use of the Random Forest we learn a mapping function f_a: $\{\boldsymbol{H}_i\} \rightarrow \{\boldsymbol{a}_i\}$.

The proposed deconvolution approach was developed as one of the stages in the image processing framework for enhancement of high-resolution retinal images [10]. In this framework, the system's noise is filtered prior to the image deconvolution stage. Therefore, here, we neglect the noise term n and assume that images are corrupted only by convolution blur kernel w.

2.2 Multi-variate Random Forest

The forest is a collection of T decision trees which are trained independently using a training dataset $U = \{\boldsymbol{H}_i, \boldsymbol{a}_i\}$. Each tree consists of non-terminal split nodes and terminal leaf nodes. The split nodes are responsible for performing a binary split on the input dataset, whereas the leaf nodes store the probability distribution of data arriving at their terminal position. At the j[th] split node, splitting function $f(U_j, \Theta)$ learns the optimal parameter $\Theta = (k, \tau)$, where k is the index of the test image feature and τ is its corresponding learned threshold defining the split. The optimal parameter Θ, that maximizes the information gain $Q(U_j, \Theta)$, is selected from a pool of randomly generated parameters. Training continues until a maximum depth D is reached or the data arriving at the j[th] node contains a minimum number of samples required for creating a leaf node.

In this work, Random Forest consisted of $T = 80$ trees with a maximum depth $D = 15$. These parameters were established by performing greedy optimization, where the root-mean-square error (RMSE) between the training $\{\boldsymbol{a}_i\}$ and predicted PSFs $\mathbf{a}^*$ was evaluated.

In order to find an optimal split parameter Θ at j[th] split node, an objective function is defined as the information gain $Q(U_j, \Theta)$:

$$Q(U_j, \Theta) = E(U_j) - \sum_{q \in \{left, right\}} \frac{|U_j^q|}{|U_j|} E(U_j^q), \tag{3}$$

where $E(U_j) = \log\left(\frac{1}{|U_j|}\sum_{i=1}^{N}\left(\boldsymbol{a}_i^j - \overline{\boldsymbol{a}^j}\right)^2\right)$ is the multi-variate differential entropy for the target vector of Zernike coefficients $\boldsymbol{a}_i^j$ with mean $\overline{\boldsymbol{a}^j}$ of data U_j and q defines the data for child nodes.

2.3 Generation of Training Data

Since no GT data is available for AO retinal images, the Random Forest was trained on synthetically generated retinal images and blur kernels replicating the PSFs of the flood-illuminated AO system. For a training dataset U, a set of convolutional blur kernels $\{w_i\}$ was generated so as to simulate optical aberrations of the eye. Low-order aberrations such as astigmatism, defocus and prism are usually well compensated with the Badal system embedded in the AO instrument [11]. These aberrations are represented by Zernike polynomials up to 6th order (as defined by Noll [12]). Thus, the pupil phase of the PSF was expanded on Zernike polynomials of higher order aberrations, retaining terms up to 15th order. An additional term corresponding to defocus was added so as to account for residual blur coming from different layers of the retina [6]. Mathematically this model of PSF is presented as:

$$w(\varphi) = \left|\Im^{-1}\left\{P(u)\exp\left(-\mathrm{j}\left(\frac{2\pi}{\lambda l}\right)\mathrm{y\ u}\right)\exp\left(j\left(\varphi(u) + \varphi_d(u)\right)\right)\right\}\right|^2, \tag{4}$$

where P is the pupil function, λ is the central wavelength of imaging beam; l is the focal length of the optical system; y defines the coordinates of two-dimensional focal plane, $\varphi(x,y) = \sum_{m=7}^{15} a_m Z_m(x,y)$ is the wavefront phase error, $\varphi_d(x,y) = a_4 Z_4(x,y)$ is the defocus phase, a_m and Z_m are Zernike coefficients and Zernike polynomial.

The values of the Zernike coefficients were sampled from a statistical model of the wavefront aberrations in healthy eyes reported in [13]. The range of Zernike coefficients was quantized between $[mean - \frac{std}{2}, mean + \frac{std}{2}]$ with the step size of 0.01µm. In order to account for partial compensation of aberrations with the AO system, these values were scaled by 0.42 [14]. Imaging wavelength and focal plane sampling were set according to the specifications of AO instrument, rtx1 ($750\ nm$ and $1.6\ \mu m$). A pupil diameter was assigned to 6 mm and axial length to 24 mm. Since all parameters defining the PSF were fixed to constant values, the PSF of the AO system can be represented by a vector of Zernike coefficients only, i.e. $\{\boldsymbol{a}_i\}$.

In order to generate a set of synthetic blurred retinal images $\{Y_i\}$, we firstly created an ideal retinal image X, using the algorithm described in [15]. The obtained synthetic image was convolved with each PSF from the set $\{w_i\}$. HoG feature vectors were extracted around the strongest corners in small regions of size 10x10 pixels centered at photoreceptor cell locations. As the cone coordinates are known through the process of synthetic image generation, locating windows with photoreceptor cells is straightforward. In addition to distinct variations caused by different types of optical

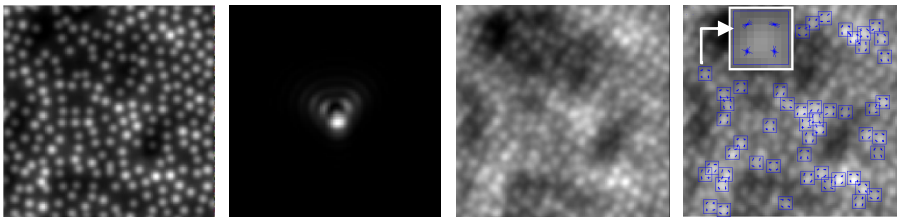

Fig. 1. Results of synthetic data generation and feature extraction, showing (a) ideal retinal image, (b) generated PSF, (c) synthetic blurred retinal image, (d) HoG features extracted from cone windows

blur, the retinal mosaic has a unique pattern, varying across the retina as well as human eyes. By extracting features from small windows containing a single cone, we limit the nature of variations down to the corruption of cone shape due to blur, thus assuring the inference of PSFs for any retinal image, taken at different locations of the retina. Moreover, due light scattering and the angle of incident light, photoreceptor cells appear with different intensity levels in the acquired image. To eliminate these variations, for each blurred image HoG features were extracted from 50 windows containing the brightest cones only. The resulting vector $\{\boldsymbol{H}_i\}$ of size 36x1 was obtained by averaging HoG features across 50 windows. Fig. 1 shows the example of synthetic data generation and image feature extraction.

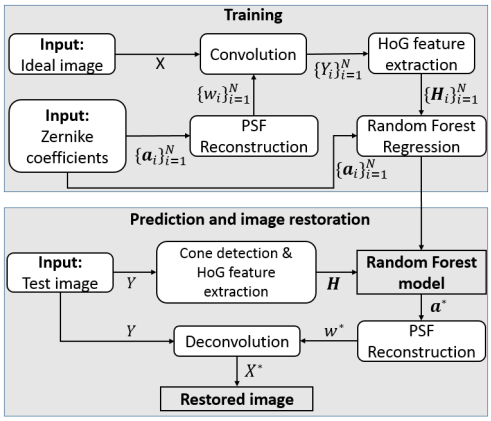

Fig. 2. Flowchart showing the process of training, prediction and image restoration

2.4 Training, Prediction and Image Restoration

Training is done offline using the training dataset: HoG feature vectors $\{\boldsymbol{H}_i\}$, extracted from a set of blurred images $\{Y_i\}$, and Zernike coefficients $\{\boldsymbol{a}_i\}$, where each vector represents a combination of different types of optical aberrations in the eye. Based on the range of values for each of the Zernike coefficients, we obtained 134,400 combi-

nations of optical PSFs. Thus, the Random Forest was trained on 134,400 synthetic blurred retinal images and blur kernels.

During the training stage, Random Forest learns the optimal split function by maximizing the information gain as defined in Eq. 3. The branches in the tree terminate with leaf nodes that contain the vectors of Zernike coefficients arriving as a result of the splitting process.

The prediction of Zernike coefficients is done online using the same feature extraction method as for the training stage. In case of real AO retinal images, the cone coordinates are found automatically, using the algorithm described in [16]. During the prediction, a given image feature vector propagates down the branches of each tree where a leaf node gives a posterior probability and the corresponding data. Kernel density estimation was used on the data aggregated from all the leaf nodes to find an optimal vector of Zernike coefficients $\boldsymbol{a}^*$ with the highest posterior probability.

After prediction, the estimated optimal vector of Zernike coefficients $\boldsymbol{a}^*$ was used to reconstruct the corresponding PSF w^*, using Eq. 4. Then, the obtained PSF was employed in the restoration of the blurred retinal image with Lucy-Richardson deconvolution algorithm [17], [18]. Fig. 2 illustrates the process of training, prediction and image restoration.

3 Results and Evaluation

3.1 Experimental Validation using Synthetic Data

To evaluate the accuracy of the PSF estimation, the synthetic dataset was divided into two subsets used for training and testing. The training set was obtained by convolving blur kernels $\{Y_i\}$ with a single uncorrupted retinal image X. To test whether the trained Random Forest has generalized well for the inference of convolution blur kernels for any retinal images, test data was generated separately. Blur kernels were produced by taking the intermediate values from the range of Zernike coefficients and reconstructing corresponding PSFs. 10 ideal retinal images X were generated so as to reproduce different retinal mosaics and convolved with 100 PSFs obtained from randomly generated vectors of Zernike coefficients. Then, the HoG features were extracted and stored for the prediction stage. Thus, the test data composed of 1000 image pairs represents the unseen data to evaluate the generalization of the Random Forest.

Fig. 3 presents few examples of the predicted PSFs, corresponding blurred images, and restored retinal images. These results are compared with GT data: the PSFs obtained from training vectors of Zernike coefficients, corresponding blurred images and uncorrupted synthetic retinal images X.

To evaluate the performance of the proposed method, quantitative assessment was performed on 1000 synthetically blurred retinal images. All images were normalized from the original range of intensities to [0,1]. The mean RMSE between the predicted convolutional blur kernels and the GT PSFs was found to be 0.0051 across 100 samples of each synthetic image X. The mean RMSE between the restored retinal images and original synthetic images across 100 samples of each test data was 0.0464. This represents 0.5% and 4.6% of generalization error correspondingly.

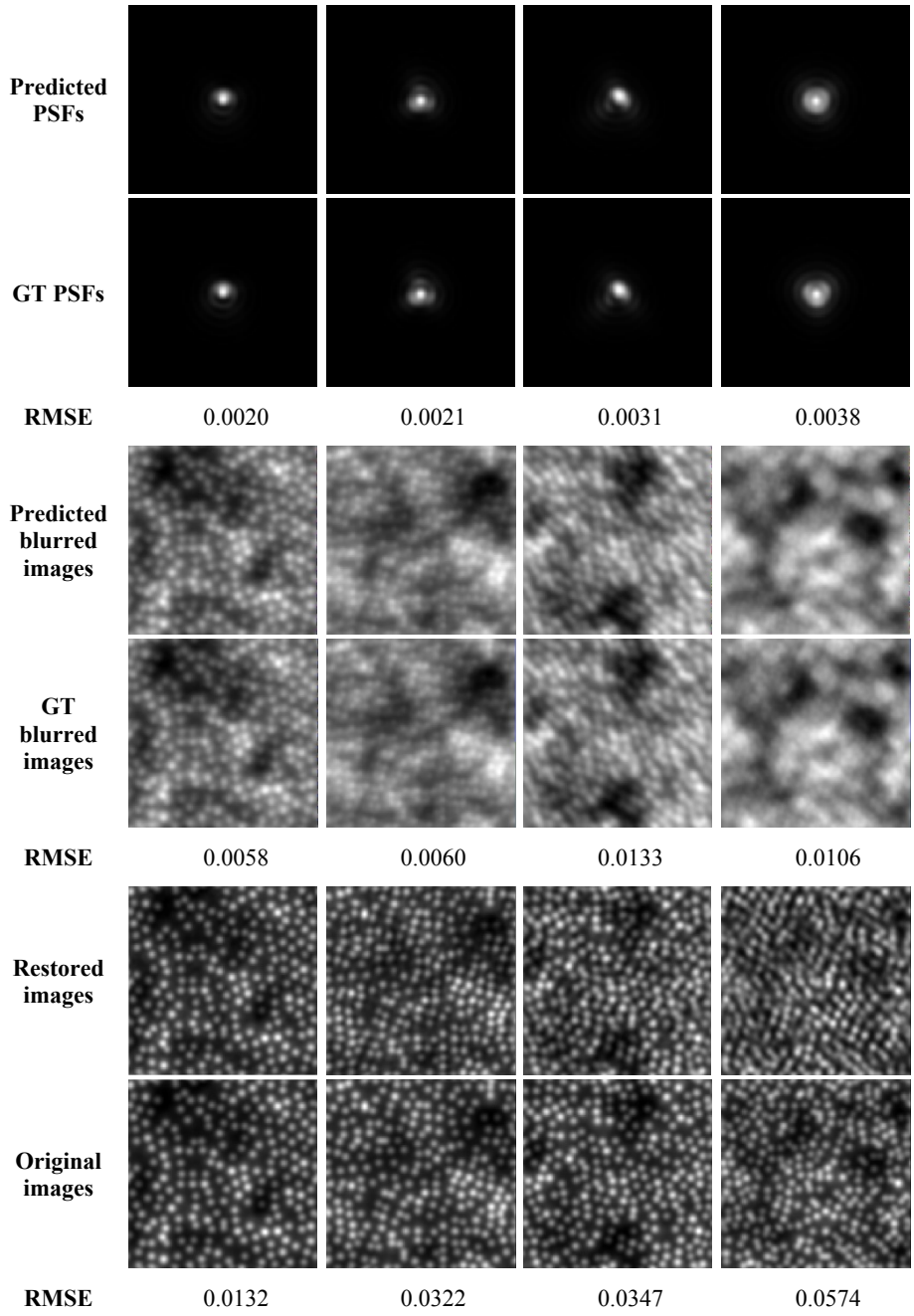

Fig. 3. Deconvolution of four representative synthetic images imitating retina at different eccentricities, showing the predicted PSFs, corresponding blurred images, images restored with the estimated PSFs and the GT data

3.2 Experimental Validation using Real AO Retinal Images

The trained Random Forest was used for predicting convolutional blur kernels for high-resolution retinal images, acquired with the flood-illuminated AO instrument in different subjects and at various eccentricities. Fig. 4-a, b shows a section of high-resolution retinal image before and after applying the proposed restoration process.

In the case of real retinal images, there is no GT data for evaluation of the results. For this reason, we assessed the performance of the proposed method in terms of image quality metrics in 25 high-resolution retinal images processed as described in [10]. Since the WFS data is not available in a commercial AO instrument, we compared the obtained results with the images restored using a blind deconvolution method of Sroubek [19]. In this method, blind deconvolution is represented as a l_1-regularized optimization problem, where a solution is found by alternately optimizing with respect to the image and kernel blurs. For a faster convergence, minimization is addressed with an augmented Lagrangian method (ALM). Based on the results of this study, the proposed method outperforms the ALM in terms of the contrast and image sharpness (Table 1). From the retinal images processed with the two methods (Fig.4-b, c), it becomes apparent that the proposed method preserves better the edges of photoreceptor cells as well as achieves better differentiation of individual cells.

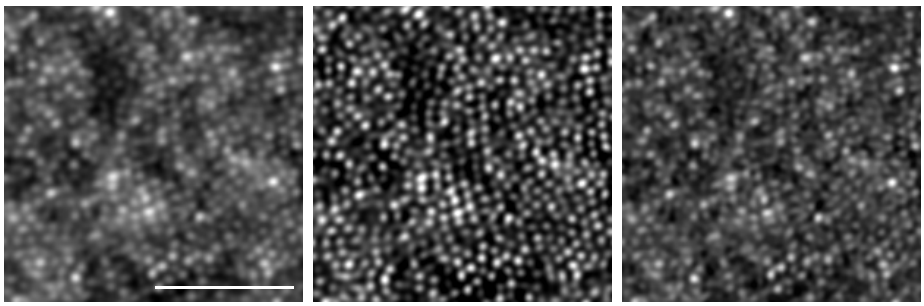

a b c

Fig. 4. Representative AO high-resolution retinal image before (a) and after restoration using the proposed approach (b) and ALM (c). The scale bar is 81 μm

Table 1. Quality assessment of the original AO retinal images before and after restoration using the proposed approach and ALM averaged for 25 images from different subjects.

	Original image	**Images restored with the proposed method**	**Images restored with the ALM method**
Image contrast	0.0216	0.0638	0.0479
Image sharpness	0.2076	0.4100	0.3601

4 Discussion and Conclusion

In this paper, we demonstrated that Random Forest regression can be used for estimating PSF of an AO imaging system. The Random Forest was trained on a large dataset by learning the mapping of HoG features, extracted from synthetically blurred retinal images onto the space of corresponding PSFs represented by Zernike coefficients. A mathematical model for the PSF was parameterized through the pupil phase, thereby significantly reducing the number of unknowns in the regression target. By extracting the information about the object shape from a single cone with the use of HoG features averaged across the image, we limited the nature of variations present in retinal images. This reduced the generalization error and allowed for the inference of PSFs from unseen images of various quality, acquired at different locations.

The validation study on synthetic data showed an average error of 0.0051 for the predicted blur kernels and 0.0464 for the reconstructed images, compared to the GT. Qualitative analysis of the results indicated that most of the errors come from images that were significantly distorted (Fig. 3, last column). In clinical practice, images with such poor quality would be rarely used for quantitative assessment of cone photoreceptor distribution. Retinal images where photoreceptor cells cannot be resolved are usually discarded from analysis or attributed to eye pathologies. While in this study the Random Forest was trained on the model of healthy eyes, in case of pathological retinas a different model might be required for setting the range of values of Zernike coefficients.

The obtained results proved that the proposed approach is applicable for the enhancement of real retinal images. For validation purposes, a comparison analysis was performed using 25 retinal images restored with the proposed method and ALM. The results demonstrated that the method based on Random Forest regressor provides higher image contrast and sharpness than the ALM (Table 1) as well as achieves a better differentiation of photoreceptor cells. However, the proposed approach could not always restore the regularity of photoreceptor cell shape. This can be attributed to the limitations of the proposed method, such as fixed axial length and pupil diameter as well as compensation of aberrations up to 15^{th} order Zernike polynomials. Despite these limitations, the Random Forest is still able to generalize to most cases. This shows the promise of the proposed method, where more complex blur kernels can be modeled. We aim to address this in our future work.

5 References

1. Rao, C., Yu, T., Hua, B.: Topics in Adaptive Optics. AO-Based High Resolution Image Post-Processing. In: Tyson, R. K. (eds.) Topics in Adaptive Optics., pp. 69–94, InTech (2012)
2. Arines, J.: Partially compensated deconvolution from wavefront sensing images of the eye fundus. Opt. Commun., vol. 284, no. 6, pp. 1548–1552 (2011)
3. Christou, J. C., Roorda, A., Williams, D. R.: Deconvolution of adaptive optics retinal images. J. Opt. Soc. Am. A. Opt. Image Sci. Vis., vol. 21, no. 8, pp. 1393–401 (2004)

4. Blanco, L., Mugnier, L. M.: Marginal blind deconvolution of adaptive optics retinal images. Opt. Express, vol. 19, no. 23, p. 23227 (2011)
5. Li, H., Lu, J., Shi, G., Zhang, Y.: Real-time blind deconvolution of retinal images in adaptive optics scanning laser ophthalmoscopy. Opt. Commun., vol. 284, no. 13, pp. 3258–3263 (2011)
6. Chenegros, G., Mugnier, L. M., Lacombe, F., Glanc, M.: 3D phase diversity: a myopic deconvolution method for short-exposure images: application to retinal imaging. J. Opt. Soc. Am. A, vol. 24, no. 5, p. 1349 (2007)
7. Fanello, S. R., Keskin, C., Kohli, P., Izadi, S., Shotton, J., Criminisi, A., Pattacini, U., Paek T.: Filter Forests for Learning Data-Dependent Convolutional Kernels. In: IEEE CVPR, pp. 1709–1716 (2014)
8. Schuler, C. J., Burger, H. C., Harmeling, S., Scholkopf, B.: A Machine Learning Approach for Non-blind Image Deconvolution. In: IEEE CVPR, pp. 1067–1074 (2013).
9. Dalal, N., Triggs B.: Histograms of Oriented Gradients for Human Detection. In: CVPR, vol. 1, pp. 886-893 (2005).
10. Lazareva, A., Liatsis, P., Rauscher, F. G.: An automated image processing system for the detection of photoreceptor cells in adaptive optics retinal images. In: IWSSIP, pp. 196–199 (2015)
11. Atchison, D. A., Bradley, A., Thibos, L. N., Smith, G.: Useful variations of the Badal Optometer. Optom. Vis. Sci., vol. 72, no. 4, pp. 279–84 (1995)
12. Noll, R. J.: Zernike polynomials and atmospheric turbulence. J. Opt. Soc. Am., vol. 66, no. 3, p. 207 (1976)
13. Thibos, L. N., Bradley, A., Hong, X.: A statistical model of the aberration structure of normal, well-corrected eyes. Ophthalmic Physiol. Opt., vol. 22, no. 5, pp. 427–33, (2002)
14. Valeshabad, A. K., Wanek, J., Grant, P., Lim, J. I., Chau, F. Y., Zelkha, R., Camardo, N., Shahidi, M.: Wavefront error correction with adaptive optics in diabetic retinopathy. Optom. Vis. Sci., vol. 91, no. 10, pp. 1238–43 (2014)
15. Mariotti L., Devaney, N.: Performance analysis of cone detection algorithms. J. Opt. Soc. Am. A, vol. 32, no. 4, p. 497 (2015)
16. Lazareva, A., Liatsis, P., Rauscher, F. G.: Hessian-LoG filtering for enhancement and detection of photoreceptor cells in adaptive optics retinal images. J. Opt. Soc. Am. A, vol. 33, no. 1, p. 84 (2015)
17. Lucy, L. B.: An iterative technique for the rectification of observed distributions. Astron. J., vol. 79, p. 745 (1974)
18. Richardson, W. H.: Bayesian-Based Iterative Method of Image Restoration. J. Opt. Soc. Am., vol. 62, no. 1, p. 55 (1972)
19. Sroubek, F., Milanfar, P.: Robust multichannel blind deconvolution via fast alternating minimization. In: IEEE Trans. Image Process., vol. 21, no. 4, pp. 1687–700 (2012)